

This discussion paper is/has been under review for the journal Hydrology and Earth System Sciences (HESS). Please refer to the corresponding final paper in HESS if available.

# Evaluation of an extreme-condition-inverse calibration remote sensing model for mapping energy balance fluxes in arid riparian areas

S.-H. Hong<sup>1,\*</sup>, J. M. H. Hendrickx<sup>1</sup>, J. Kleissl<sup>2</sup>, R. G. Allen<sup>3</sup>,  
W. G. M. Bastiaanssen<sup>4</sup>, R. L. Scott<sup>5</sup>, and A. L. Steinwand<sup>6</sup>

<sup>1</sup>New Mexico Tech, Socorro, NM, USA

<sup>2</sup>University of California, San Diego, CA, USA

<sup>3</sup>University of Idaho, Kimberly, ID, USA

<sup>4</sup>Delft University of Technology, Delft, the Netherlands

<sup>5</sup>Southwest Watershed Research Center, USDA-ARS, Tucson, AZ, USA

<sup>6</sup>Inyo County, Water Department, Independence, CA, USA

\*now at: Murray State University, Murray, KY, USA

13479

Received: 22 August 2014 – Accepted: 17 November 2014 – Published: 10 December 2014

Correspondence to: S.-H. Hong (shong4@murraystate.edu)

Published by Copernicus Publications on behalf of the European Geosciences Union.

13480

Discussion Paper

Discussion Paper

Discussion Paper

Discussion Paper

Discussion Paper

Discussion Paper

Discussion Paper

Discussion Paper



region of interest; unlike NLDAS and LIS, SEBAL and METRIC do not require land cover maps. However, applications of SEBAL and METRIC are restricted to clear days over areas of unvarying weather, and require some supervised calibration for each image, preventing application at the continental scale such as done by ALEXI, SSEB, MOD16, NLDAS and LIS.

The accuracy of SEBAL and METRIC for evaporation mapping worldwide is typically about  $\pm 15$  and  $\pm 5$  % for, respectively, daily and seasonal evaporation estimates (Bastiaanssen et al., 2005; Allen et al., 2011). Such accuracy is obtained by a calibration method that selects a “cold” and “hot” pixel representing extreme thermal and vegetation conditions within an image. After calculation of the energy balance at the two calibration pixels the sensible heat flux  $H$  for each pixel is indexed to its satellite measured surface temperature. The economic efficiency of SEBAL and METRIC is remarkable. For example, in the early 1980's co-author Hendrickx was deployed at Niono in the Office du Niger in Mali to determine water requirements for flood irrigated rice. It took him and a team of four field assistants and several graduate students more than two years to measure the seasonal actual evapotranspiration of rice in four irrigation units covering a total area of about 70 ha using non-weighing lysimeters and discharge measurement structures in irrigation and drainage ditches (Hendrickx et al., 1986). In 2008, the seasonal actual evapotranspiration was obtained for all 86 000 ha of the Office du Niger using SEBAL with Landsat imagery of 2006 at an effort of about two expert months without need for an overseas multi-year deployment (Zwart and Leclert, 2010).

Previous validation studies of SEBAL have mainly been conducted in relatively homogeneous agricultural areas and have focused on comparison of daily ET rates estimated from SEBAL and METRIC with ground measurements using lysimeters (Tasumi, 2003; Trezza, 2002), Bowen ratio and eddy covariance methods (Gibson et al., 2013; Du et al., 2013; Bastiaanssen et al., 2002) and scintillometry (Hemakumara et al., 2003; Kite and Droogers, 2000; Kleissl et al., 2009). The overall goal of this study is to conduct a thorough evaluation of the performance of SEBAL in arid riparian areas

13483

in New Mexico, Arizona and California. Here, vast deserts are transected by narrow river valleys covered by a mosaic of irrigated agricultural fields and riparian vegetation (cottonwood, saltcedar, willow, mesquite, Russian olive and salt grasses) which creates a very heterogeneous landscape with a short patch length scale. If SEBAL performs well under these challenging conditions, it is likely to perform well in most arid and semi-arid regions. Another difference with previous studies is our focus on all components of the energy balance during the instant of satellite overpass as well as on a daily basis. We can accomplish this since we have available a quality controlled data set consisting of  $R_n$ ,  $H$  and LE measurements in the riparian areas of the Middle Rio Grande Basin (New Mexico) and  $R_n$ ,  $G$ ,  $H$  and LE measurements in the riparian areas of the San Pedro Basin (Arizona) and the Owens River Valley (California).

## 2 Surface Energy Balance Algorithm for Land (SEBAL)

SEBAL is a remote sensing algorithm that evaluates the fluxes of the energy balance and determines LE as the residual

$$LE = R_n - G - H \quad (1)$$

where  $R_n$  is the net radiation flux density [ $\text{W m}^{-2}$ ],  $G$  is the soil heat flux density [ $\text{W m}^{-2}$ ],  $H$  is the sensible heat flux density [ $\text{W m}^{-2}$ ], and  $LE (= \lambda ET)$  is the latent heat flux density [ $\text{W m}^{-2}$ ], which can be converted to the ET rate [ $\text{mm day}^{-1}$ ] using the latent heat of vaporization of water  $\lambda$  [ $\text{J kg}^{-1}$ ] and the density of water  $\rho_w$  [ $\text{kg m}^{-3}$ ].

To implement SEBAL, images are needed with information on reflectance in the visible, near-infrared and mid-infrared bands as well as emission in the thermal infrared band. Such images are offered by a number of satellites such as Land Satellite (Landsat), Moderate Resolution Imaging Spectroradiometer (MODIS), Advanced Very High Resolution Radiometer (AVHRR), Advanced Spaceborne Thermal Emission and Reflection Radiometer (ASTER), ENVISAT-Advanced Along Track Scanning Radiometer

13484







sonable agreement found between SEBAL derived instantaneous soil heat fluxes and those measured on the ground in the Owens and San Pedro River Valleys (Table 5). If the sum of  $H$  and  $LE$ , before correction, was less than 65 % or greater than 110 % of the available energy ( $R_n - G$ ), the data were not used in our analysis. This criterion  
5 leads to the exclusion of 45 % of instantaneous fluxes and 39 % of the daily fluxes of the data from the Middle Rio Grande Valley, 79 % (instantaneous) and 43 % (daily) from the Owens River Valley and 17 % (instantaneous) and zero % (daily) from the San Pedro River Valley. The remaining turbulent heat flux estimates are improved thru forcing the closure of the energy balance by increasing  $LE$  and  $H$  by the Bowen ratio (Twine  
10 et al., 2000). The improved adjusted  $H$  and  $LE$  are identified as  $H_{adj}$  and  $LE_{adj}$ .

After elimination of EC measurements on the basis of unacceptable closures, we eliminated also the EC measurements taken on 16 May 2003 in the San Pedro River Valley at the Mesquite (CM) site. On this day the wind direction was approximately  $90^\circ$  different from the prevailing wind direction which resulted in fetch distances considerably shorter than the recommended 100 times the sensor height above the canopy  
15 (Stannard, 1993; Sumner and Jacobs, 2005). The problem was exacerbated by the relatively high placement (7 m) of the sensors above the canopy (Table 2) since the heat fluxes can vary significantly with height under such conditions (De Bruin et al., 1991).

### 3.3 Comparison of SEBAL flux predictions to ground measurements

20 Comparison of SEBAL derived estimates of  $R_n$ ,  $G$ ,  $H$  and  $LE$  with ground measurements is not a straightforward operation because the spatial and temporal scales of the SEBAL predictions and ground measurements are quite different. In this section we will discuss these scale gaps for each flux in the energy balance.

#### 3.3.1 Net radiation

25  $R_n$  is measured with a net radiometer at a height of about 2–3 m above the canopy (Table 2) that covers typically an observation area on the order of  $10\text{ m}^2$ . The measure-

13491

ments are taken every second and made available as 30 min averages for this study. The SEBAL  $R_n$  prediction is derived from reflectances in the visible, near-infrared and mid-infrared bands from a  $900\text{ m}^2$  pixel as well as the emittance in the thermal band from a  $3600\text{ m}^2$  pixel. Thus, the  $R_n$  ground observation is based on a measurement  
5 area at least two orders of magnitude smaller than the SEBAL prediction. For homogeneous areas this difference will not matter much but for heterogeneous areas it may cause serious bias, since the satellite based  $R_n$  samples a larger area and is therefore more representative of the EC footprint. In riparian areas heterogeneity is the rule rather than exception. Radiometers are typically placed over the canopy of interest  
10 which may cause under-representation of surrounding bare soil or ground cover in the angle of view. Therefore, ground measured  $R_n$  is expected to be biased towards the  $R_n$  of the vegetation of interest.

#### 3.3.2 Soil heat flux

$G$  is measured by soil heat flux plates combined with the determination of changes in heat storage above the plate using soil temperature and soil water content measurements.  
15 If  $G$  is not corrected for heat storage above the plate, large errors will result (Sauer, 2002a). This is the case for the measurements at the Middle Rio Grande sites and, therefore, these  $G$  measurements have not been used for the comparison. The measurement area of a soil heat flux plate is about  $0.001\text{ m}^2$  which is almost six orders of magnitude less than a  $900\text{ m}^2$  Landsat pixel.  $G$  is spatially variable due to  
20 heterogeneity in soil moisture and vegetation cover, so that numerous flux measurements would be needed to estimate the average pixel  $G$  with the desired accuracy (Kustas et al., 2000; Humes et al., 1994). Therefore, we expect the instantaneous  $G$  ground measurements to be a rather crude estimation of the true instantaneous  
25  $G$  of a pixel. The instantaneous  $G$  can vary widely depending on soil condition ( $20\text{--}300\text{ W m}^{-2}$ ) (Sauer et al., 2003). Since  $G$  is positive during the day and negative during the night the daily  $G$  is rather small compared to the other components of the energy

13492

balance (Seguin and Itier, 1983).  $G$  is measured in the field every second; we used averages of 30 min for this study.

### 3.3.3 Sensible and latent heat fluxes

$H$  and LE are measured using a three-dimensional sonic anemometer-thermometer and Krypton hygrometer, respectively (or open patch infrared gas analyzer). For these components of the energy balance the relationship between ground measurement area and pixel size is the opposite of the one discussed for  $R_n$  and  $G$ : the area of ground measurements is several times larger than a Landsat pixel. As discussed in Sect. 3.4 a typical footprint for  $H$  and LE under the micrometeorological conditions of this clear-sky study covers about 5 pixels or about 4500 m<sup>2</sup>. The location of the footprint is upwind of the EC tower and its size and distance from the tower depends on atmospheric stability. For the comparison of  $H$  and LE SEBAL estimates with ground measurements, first the footprint area must be determined and then, the weighted average is taken of the SEBAL estimated  $H$  and LE values of all pixels within the footprint area. These weighted averages of  $H$  and LE are compared with the ground measured  $H$  and LE at the EC tower. This approach is expected to work reasonably well for comparison of SEBAL instantaneous  $H$  and LE estimates with ground measurements at the time of the satellite overpass.

Comparison of daily  $H$  and LE fluxes is problematic. Instantaneous  $H$  and LE measurements are available at the EC tower as 30 min averages but SEBAL estimates of the instantaneous  $H$  and LE are only available once per image day at the time of the satellite overpass. Therefore, it is impossible to compare every 30 min the footprint averaged SEBAL estimates with the ground measurements. It is also problematic to compare daily SEBAL estimates of  $H$  and LE at each pixel with daily  $H$  and LE measurements at the EC tower. Daily  $H$  and LE measurements at the EC tower are the daily sum of 30 min instantaneous  $H$  and LE measurements originating from different footprints covering a wide area especially on days with highly variable wind directions. Combining the assumption of constant evaporative fraction during the day with the daily

13493

footprint using daily-averaged parameters including air temperature,  $u^*$ , wind speed and direction, it may be possible to compare daily  $H$  and LE measurements at the tower with SEBAL estimates. However, uncertainties would remain and at best a rough comparison can be made since the average daily values are not necessarily a good measure for determination of a daily footprint. Therefore, in this study rather than trying to determine the true location of the “representative” daily foot print, the daily  $H$  and LE ground measurements will be compared with the average SEBAL estimated  $H$  and LE fluxes originating from twenty-five homogeneous pixels surrounding the EC tower. The homogeneity of the pixels surrounding the tower was evaluated by inspecting NDVI, albedo, and surface temperature values as well as the  $H$  and LE values themselves.

### 3.3.4 Quantitative measures to compare SEBAL estimates and ground measurements

The numerical comparison of the energy balance components ( $R_n$ ,  $G$ ,  $H$ , and LE) estimated by SEBAL with those measured on the ground is conducted by means of quantitative measures proposed by Willmott and others for the validation of atmospheric models (Willmott, 1981, 1982; Fox, 1981). We use the coefficient of determination ( $r^2$ ), mean absolute difference (MAD), root mean square difference (RMSD), and the mean relative difference (MRD) (Hong, 2008). The coefficients of determination may be misleading as “high” or statistically significant values of  $r$  are often unrelated to the sizes of the differences between model estimates and measurements (Willmott and Wicks, 1980). In addition, the distributions of the estimates and measurements will often not conform to the assumptions that are prerequisite to the application of inferential statistics (Willmott, 1982). However, since  $r^2$  is a commonly used correlation measure that reflects the proportion of the “variance explained” by the model, we report this measure. The MAD and RMSD are robust measures as they summarize the mean differences between SEBAL estimates and ground measurements; the MAD is less sensitive to outliers than RMSD. The MRD is often used as an indication how well SEBAL estimates agree with ground measurements (Bastiaanssen et al., 2005).

13494



### 3.4 Footprint model

The location and extent of the footprint depends on surface roughness, atmospheric stability, wind speed, wind direction and may cover many pixels upwind of the eddy covariance tower (Schmid and Oke, 1990; Hsieh et al., 2000). There are several types of footprint models. Initially, simple two-dimensional analytical footprint models for neutral atmospheric conditions were developed (Gash, 1986; Schuepp et al., 1990). Later, the analytical footprint model was improved to account for atmospheric stability conditions (Horst and Weil, 1992; Hsieh et al., 2000). The footprint flux,  $F_{(x,z_s)}$  [-], along the upwind direction,  $x$  [m], measured at the height  $z_s$  [m], suggested by (Hsieh et al., 2000) is used in this study.

A typical footprint size and footprint intensity for one 30 min period on 19 August 2002, at a Rio Grande saltcedar EC tower is presented in Fig. 2. To verify the quality of the footprint model used in this study, we also calculated  $x_{\max}$  (peak footprint) for this period with the model by Schuepp et al. (1990). The models by Hsieh et al. (2000) and Schuepp et al. (2000) calculate  $x_{\max}$  as 10 m (Fig. 2) and 11 m, respectively, which implies that the footprint from Hsieh et al. (2000) is indeed close to the tower. At most EC sites, the maximum contribution to the footprint was within 50 m from the tower (wind speeds were generally less than  $4 \text{ ms}^{-1}$ ) and most of the footprint intensity (> 90 %) is located within 300 m from the tower. We compute the footprints from meteorological parameters including air temperature, sensible heat flux, wind speed, wind direction and friction velocity. The footprints for  $H$  and LE are obtained for the time of the satellite overpass using the 30 min averaged meteorological parameters. Approximately 80 % of all footprint fluxes cover an area of 5 to 9 pixels, twenty percent cover larger areas. As explained in Sect. 3.3.3 calculation of a representative daily footprint for comparison of SEBAL  $H$  and LE estimates and ground measurements is nearly impossible. Therefore, the use the average  $H$  and LE values of the 25 pixels surrounding the EC tower pixel is considered to be the best option for the comparison of daily ground measurements and SEBAL estimates.

13495

### 3.5 Calibration and evaluation of SEBAL flux predictions

This study cannot be a robust validation study due to missing soil heat flux measurements in the Middle Rio Grande Valley and biased net radiation measurements over heterogeneous riparian vegetation with patches of bare soil. Our aim is to evaluate the challenges of SEBAL flux predictions in arid riparian areas using a validation approach.

Calibration is the process of adjusting hydrologic model parameters to obtain a fit to observed data. In SEBAL the relationship between model parameter  $\Delta T$  and remotely observed radiometric surface temperature  $T_s$  in Eq. (4) is calibrated using the remotely observed energy balance components of  $R_n$  and  $G$  at two extreme conditions in a Landsat image: the cold wet pixel and hot dry pixel.

After calibration, validation tests typically are applied to a second set of data to test the performance of a hydrologic model. In the context of this study the second data set consists of ground measurements of  $R_n$ ,  $G$ ,  $H$  and LE, at pixels other than the cold and hot pixels. Validation or evaluation is accomplished by comparing the SEBAL predicted energy balance components with the ones measured on the ground at locations with eddy covariance towers.

#### Calibration approaches

The temperatures of the cold and hot pixel for the derivation of calibration coefficients  $c_1$  and  $c_2$  in Eq. (4) are most critical in SEBAL as well as METRIC since they constrain LE between its maximum value at the cold wet pixel and zero at the hot dry pixel by reducing biases in  $H$  associated with uncertainties in aerodynamic characteristics including  $T_s$  (Bastiaanssen et al., 2005; Allen et al., 2006). In SEBAL this calibration is entirely based on information that is available inside the image and, therefore, it is called “self-calibration” (Bastiaanssen et al., 2005) or “internalized calibration” and “autocalibration”.

Over the cold pixel it is assumed that  $\Delta T = 0$ , which implies that  $H = 0$  and  $\text{LE} = R_n - G$ . An alternative manner in METRIC is to use high quality hourly meteorological

13496

observations for the calculation of the reference ET (Allen et al., 1998) for the estimation of  $H$  in well-irrigated alfalfa and clipped grass fields (Allen et al., 2007, 2011). However, this study deals with a SEBAL application in riparian areas without high quality hourly meteorological observations as is the default condition for many regions worldwide (Droogers and Allen, 2002). The selection of the hot pixel is quite challenging because the heterogeneous landscapes of the southwestern US include quite a few hot and dry areas with a wide range of temperatures. In this study, the hot pixel is selected from a dry bare agricultural field where ET is just close to zero. Therefore, for any pixel cooler than the hot pixel,  $ET > 0$  (if the  $R_n$  and  $G$  are the same), and for any pixel warmer than the hot pixel, for example a parking lots,  $ET = 0$ . In addition, the equation for  $G$  estimation was derived for agricultural conditions and therefore produces more dependable estimates for calibration when applied to a bare, agricultural soil having a tillage history.

As a consequence of the “internalized calibration” any biases in  $R_n$  or  $G$  at the hot pixel in the image are transferred into  $H$ . However, this bias introduced into  $H$  is transferred back out of the energy balance during the calculation of LE from Eq. (1), since the bias is present in both  $R_n - G$  and  $H$ , and thus cancels (Allen et al., 2006). The “internalized calibration” results in the least biased LE if the cold and hot pixel are properly selected and is the most distinctive feature of SEBAL and METRIC compared to other remote sensing LE algorithms.

The selection of cold and hot pixel requires a thorough understanding of field micrometeorology and is somewhat subjective, i.e. different experts will select slightly different temperature values. The cold pixel is selected where areas with well-watered healthy crops with full soil cover or in shallow water bodies (Allen et al., 2011; Bastiaanssen et al., 2005) and is relatively straightforward while the hot pixel selection is more challenging. Therefore, it has been proposed to use micrometeorological ground measurements of energy balance components for the calibration and validation of remote sensing algorithms such as SEBAL (Kleissl et al., 2009). However, due to the relatively large uncertainties of ground measured sensible and latent heat fluxes (Loescher

13497

et al., 2005; Kleissl et al., 2008) the value of ground measurements for calibration of SEBAL is not well established. For this reason we test two different calibration approaches for the selection of the temperatures for the cold and hot pixel: the *Empirical* (EM) approach and the *Eddy Covariance* (EC) approach. The former is based on inspection of the hydrogeological features of the landscape and qualitative micrometeorological considerations and is typical for most SEBAL applications since the high number of EC towers available in this study is a unique situation. The Eddy Covariance (EC) approach is based on inspection of the hydrogeological features of the landscape followed by fine-tuning the parameters  $c_1$  (slope) and  $c_2$  (intercept) in Eq. (4) using ground measurements of instantaneous latent heat fluxes at the EC towers after adjustment for closure error. Since selection of the cold pixel is straightforward in fully vegetated fields, the temperature of the cold pixel was fixed but the temperature of the hot pixel was varied to best match the instantaneous ground measurements of LE (Hong, 2008). In order to independently evaluate the EM vs. the EC approach, senior author Hong implemented the EC approach, while co-author Hendrickx implemented the EM approach.

Five different calibration scenarios (S1–S5) were implemented and compared (Table 3). In the EC approach, calibration of SEBAL to ground measurements was implemented either using the average footprint weighted instantaneous SEBAL LE heat fluxes (S1, EC\_FP) or using the instantaneous SEBAL LE heat flux of the pixel where the EC tower is located (S2, EC\_TP). The former method is difficult to implement for most practitioners while the latter is practical and fast but requires homogeneous conditions around the tower to the maximum extent of the footprint. The EM approach (S3) was implemented without using the LE’s measured by the EC towers or any other meteorological measurements.

In Sect. 3.3.1 it was hypothesized that the ground measured  $R_n$  may be biased towards vegetation while the SEBAL  $R_n$  may be more representative for the true  $R_n$  of a pixel covered with vegetation and bare soil patches. In Sect. 4 strong evidence is presented that the SEBAL  $R_n$  ( $SR_n$ ) is more accurate. Therefore, we also evaluated the

13498



These differences have been quantified by comparing the SEBAL estimated instantaneous and daily net radiation for fully vegetated agricultural fields, saltcedar, and bare soils (Table 5). Whereas the measured instantaneous net radiation fluxes of fully cropped agricultural fields and saltcedar stands exceeded those of bare soils by 54 to 77 %, the daily net radiation fluxes were only 20 to 36 % larger. A typical Leaf Area Index (LAI) for saltcedar in the Middle Rio Grande Valley is about 2.5 (Cleverly et al., 2002) which indicates that bare soil is present but vegetation cover is dominant. Now let us assume a typical mixed pixel with a soil cover of 75 % saltcedar and 25 % bare soil. The data from Table 5 for the first saltcedar plot show that the ratios between 100 % saltcedar and 100 % bare soil for, respectively, instantaneous and daily net radiation are 1.77 and 1.34. We want to find similar ratios between 100 % saltcedar and our mixed pixel using the values of Table 5 for the instantaneous and daily net radiation for saltcedar and bare soil. Ignoring the effect of thermal radiation from soil that is intercepted by adjacent vegetation, the instantaneous and daily net radiations for the mixed pixel are, respectively,  $0.75 \times 670 + 0.25 \times 379 = 598 \text{ W m}^{-2}$  and  $0.75 \times 19.8 + 0.25 \times 14.8 = 14.9 + 3.7 = 18.6 \text{ MJ m}^{-2} \text{ day}^{-1}$ . So, the net instantaneous and daily radiations of a fully vegetated saltcedar pixel are  $670/598 = 1.12$  and  $19.8/18.6 = 1.06$  times those of our mixed pixel. The 12 % difference is similar to the MRD's of 13–15 % presented for the difference in instantaneous net radiation between ground measurements and SEBAL estimates. The 6 % difference for daily net radiation falls within error ranges of radiation measurements (Halldin and Lundroth, 1992; Field et al., 1992). Thus, the much smaller MRD for daily  $R_n$  (–2.3 to 2.9 %) compared to the MRD of instantaneous  $R_n$  (about 13 %) can be explained by environmental radiation physics and is not caused by bias in the SEBAL method for determination of instantaneous  $R_n$  or in the radiation sensors. This leads to the conclusion that the SEBAL estimated net radiation for the  $900 \text{ m}^2$  of the EC tower pixel is more representative for each site than the ground measurements with the net radiation meter preferentially positioned over a  $10 \text{ m}^2$  patch of vegetation.

13501

### 4.3 Comparison of SEBAL soil heat flux with ground measurements

The magnitude of soil heat flux  $G$  depends on surface cover, soil water content, and solar irradiance. For a moist soil beneath a plant canopy or residue layer the instantaneous  $G$  will often be less than  $\pm 20 \text{ W m}^{-2}$  (Sauer, 2002b) while a bare, dry, exposed soil in midsummer could have a day-peak in excess of  $300 \text{ W m}^{-2}$  (Fuchs and Hadas, 1973). In the Middle Rio Grande Basin during summer typical midday (10 a.m. through 2 p.m.) values of  $G$  are 104 and  $132 \text{ W m}^{-2}$  for, respectively, upland grassland and shrubs (Kurc and Small, 2004). These values demonstrate that the instantaneous  $G$  in riparian areas can be an important component of the instantaneous energy balance that needs to be taken into account. In most field soils the instantaneous  $G$  exhibits not only a temporal variability but also a large spatial variability which makes it very difficult to measure an average  $G$  for areas with the size of a typical Landsat pixel ( $30 \text{ m} \times 30 \text{ m}$ ) (Sauer, 2002b).

For this study six soil heat flux measurements were available from the Owens Valley and the San Pedro Valley. The SEBAL determined  $G$  approaches the ground measured  $G$  reasonably well (Fig. 6) but the MRD is relatively high with values of 30.9 to 32.2 % (Table 6). However, the overall impact of the relatively high MRD in instantaneous  $G$  is minor since its MAD of  $35 \text{ W m}^{-2}$  (Table 6) hovers around 6 % percent of the SEBAL predicted instantaneous net radiation and around 5 % percent of the ground measured instantaneous net radiation. The daily  $G$  is close to zero since heat enters the soil during the day but leaves the soil during the night. The daily  $G$  measurements in the field confirm this (Table 6). Therefore, it is assumed in SEBAL that the daily heat flux can be neglected, i.e.  $G$  is zero.

Given the high spatial and temporal variability of  $G$  (Sauer, 2002b) within one Landsat pixel, the reasonable agreement between SEBAL predicted instantaneous  $G$  and ground measurements (Fig. 6 and Table 6), the relatively minor impact of an error in  $G$  on the estimates of ET, and the impossibility to measure a truly representative  $G$  for a  $900 \text{ m}^2$  heterogeneous riparian pixel using soil heat flux plates with a foot print of only

13502



instantaneous LE measurements at the EC towers. This leads to quite different  $H$  and LE SEBAL estimates in S1, S2 and S4.

In scenarios S1 and S2 of Table 7 there is no significant difference between the SEBAL estimated sensible ( $156$  vs.  $138 \text{ W m}^{-2}$ ) and latent ( $314$  vs.  $333 \text{ W m}^{-2}$ ) heat fluxes. Thus, SEBAL calibrations based on the instantaneous latent heat flux of the tower pixels (S2) or on the latent heat flux of the instantaneous foot prints during the satellite's overpass (S1) yield similar results in this study except that the MAD and RMSD of S1 are lower: MAD/RMSD values for S1 and S2 are 39/57 and 56/74, respectively. This finding is relevant for practitioners who need to calibrate SEBAL on a routine basis and/or in nearly real-time: using only the tower pixels is much faster and easier to implement automatically than determination of a footprint weighted average. It also justifies the omission of footprint scenario S1 from further consideration in scenario S4. However, for posterior SEBAL analyses and research applications use of the footprint is still recommended since (1) it results in somewhat smaller comparison measures (Table 7) and (2) footprint analyses are effective for the detection of unusual environmental conditions.

The MAD and RMSD of the sensible heat fluxes for S1, S2 and S3 are quite similar but rather high with MAD/RMSD values of, respectively, 108/131, 126/147 and 111/135. The values of S4 and S5 36/46 and 61/77 are considerably lower and reflect the ground energy balance correction by using the SEBAL net radiation. The MAD/RMSD values of the latent heat fluxes are increasing from a low value of 39/57 for S1, 56/74 for S2 to 66/81 for S3 while the values for S4 and S5 are, respectively, 39/48 and 61/77. Thus, using the net radiation correction has a much smaller effect for the latent heat fluxes than for the sensible heat fluxes which is a result of the internal calibration of SEBAL. The comparison measures for S3 and S5 (the empirical traditional SEBAL approach) are also very similar for the latent heat flux but are reduced in half for the sensible heat flux after net radiation correction.

Through the "anchoring" of  $H$  and LE at the cold and hot pixels SEBAL reduces or cancels biases introduced in the calculation of albedo, net radiation, and surface tem-

13505

perature as well as errors in narrow band emissivity, atmospheric correction, satellite sensor, aerodynamic resistance, and soil heat flux function. This can result in a reduction of total bias in ET of as much as 30% compared to other models that are not routinely internally calibrated (Allen et al., 2006). Allen et al. (2007) describe how METRIC, through the use of weather based reference ET, is able to eliminate most internal energy balance component biases at both the cold and hot extreme conditions. SEBAL, on the other hand, eliminates biases at the hot extreme, but necessarily retains a bias at the cold extreme where it is assumed that  $LE = R_n - G$ . The cost for the improved estimates for LE is a deterioration of the SEBAL and METRIC  $H$  estimates since the sensible heat flux, as an intermediate parameter, absorbs most of the aforementioned biases as a result of the internal calibration process (Choi et al., 2009).

The same trends observed in the MAD and RMSD values are found in the MRD values presented in Table 7. A striking feature in S1–S3 is the very poor prediction of the sensible heat flux with MRD's between 35 and 47%. Especially, for S1 and S2 that have been calibrated against ground measured instantaneous latent heat fluxes, this result was not expected. The discrepancy is not caused by any error in the SEBAL procedure but by the apparent bias in the ground measurements of the net radiation that was reported earlier (see Sect. 4.2). When the ground measured net radiation is replaced with the arguably more accurate SEBAL estimate of net radiation, the SEBAL estimates of sensible heat fluxes improve dramatically with MRD's in S4 and S5 of, respectively, 0.8 and 16.6%. Despite the poor MRD's of  $H$  (35 to 47%) in S1–S3 the SEBAL LE estimates exhibit good MRD's (2.7 to  $-11.5\%$ ). Therefore, these numbers provide an instructive demonstration of the power of SEBAL's internal calibration.

We conclude that calibrating SEBAL with reliable ground measurements at the pixel scale will indeed improve its estimates of both, sensible and latent instantaneous heat fluxes. However, ground measurements of sensible heat fluxes should be used cautiously and carefully for the calibration and evaluation of SEBAL, since the SEBAL sensible heat flux is biased necessarily to compensate for bias in  $R_n$ ,  $G$  and aero-

13506



## 5 Conclusions

In this study we have evaluated the SEBAL extreme-condition-inverse calibration remote sensing model in arid riparian areas by comparing its predicted instantaneous and daily energy balance components with those measured on the ground with the eddy covariance method.

An analysis of differences in instantaneous  $R_n$  during late morning (Landsat overpass time) between vegetation and exposed soil emphasizes the large impact of soil in the  $R_n$  view, and the importance of proper vegetative mixture viewed by the  $R_n$  sensor. We argue that tower  $R_n$  is generally biased toward vegetation, resulting in higher  $R_n$  values. Instantaneous  $R_n$  from SEBAL, representing a larger area for heterogeneous vegetation than the net radiometer, gives lower  $R_n$  values. When these are used to close the eddy covariance energy balance, LE and  $H$  from SEBAL and LE and  $H$  from the ground based EC are much more similar. The daily net radiation values of SEBAL agree well with the ground measurements (Table 4 and Fig. 5) as expected after examination of the daily radiation balance of mixed riparian pixels in Sect. 4.2.

The instantaneous soil heat flux values of SEBAL were about 30 % higher than the ground measured values in the San Pedro and Owens Valleys (Table 6 and Fig. 6). However, this large relative difference has a relatively minor impact on the overall energy balance since its MAD of  $35 \text{ W m}^{-2}$  (Table 6) hovers around 6 % percent of the SEBAL predicted instantaneous net radiation and around 5 % percent of the ground measured instantaneous net radiation. The daily  $G$  is close to zero since heat enters the soil during the day but leaves the soil during the night (Table 6). Therefore, it can be assumed in SEBAL that the daily heat flux is zero.

The instantaneous latent heat flux values of SEBAL were within  $-13.2$  to  $2.7$  % of the ground measurements for the five scenarios S1–S5 (Table 7 and Fig. 9). The magnitude of these differences is similar to the variability common to eddy covariance flux measurements, i.e. it is nearly impossible to decide whether these differences are a result of bias in SEBAL or the eddy covariance method. Therefore, we conclude that

13509

the SEBAL latent heat fluxes in this study over heterogeneous arid riparian areas are similar to the ones measured at the eddy covariance towers.

The instantaneous sensible heat flux values of SEBAL differ from the ground measurements by 35.0 to 47.2 % in scenarios S1, S2 and S3 but after replacing the biased ground measurement of net radiation by the SEBAL net radiation the differences reduce to 0.8 and 16.6 % for, respectively, scenarios S4 and S5. As has been explained in Sect. 4.4.1 the SEBAL sensible heat fluxes are biased since as a result of the extreme-condition-inverse internal calibration of SEBAL the sensible heat flux absorbs all biases that may occur during the SEBAL implementation.

In terms of daily sensible and latent heat fluxes, better agreement exists between ground measurements and SEBAL estimates with mean MRD's for the three scenarios range from 13.8 to  $-0.7$  %. That is because the daily net radiations measured on the ground and determined by SEBAL agree well (Table 8 and Figs. 11 and 12). Note that the use of a multiplier on the instantaneous evaporative fraction of 1.1 to convert the instantaneous ET to daily ET is preferred for the non-advective conditions during the months April to September that were covered during this study.

An important conclusion of the comparisons between various calibration strategies for SEBAL is that ground measurements of sensible heat fluxes should be used with caution for the calibration and validation of SEBAL, since the SEBAL sensible heat flux is intentionally biased during calibration (to produce an unbiased LE) and will deviate from the ground measured sensible heat flux in order to arrive at unbiased estimates of LE.

For all five calibration scenarios, the comparison measures ( $r^2$ , MAD, RMSD and MRD) of the instantaneous and daily latent heat fluxes are strong evidence that the great strength of the SEBAL and METRIC method is its internal calibration procedure that eliminates most of the bias in latent heat flux at the expense of increased bias in sensible heat flux. We conclude that SEBAL is an effective tool for mapping actual evapotranspiration at high spatial resolutions in heterogeneous riparian areas where no high-quality hourly weather data are available.

13510







- Hsieh, C.-I., Katul, G. G., and Chi, T.-W.: An approximate analytical model for footprint estimation of scalar fluxes in thermally stratified atmospheric flows, *Adv. Water Resour.*, 23, 765–772, 2000.
- Humes, K. S., Kustas, W. P., Moran, M. S., Nichols, W. D., and Wertz, M. A.: Variability of emissivity and surface temperature over a sparsely vegetated surface, *Water Resour. Res.*, 30, 1299–1310, 1994.
- Jacob, F., Olioso, A., Gu, X. F., Su, Z., and Seguin, B.: Mapping surface fluxes using airborne visible, near infrared, thermal infrared remote sensing data and a spatialized surface energy balance model, *Agronomie*, 22, 669–680, doi:10.1051/agro:2002053, 2002.
- Jiang, L. and Islam, S.: Estimation of surface evaporation map over southern Great Plains using remote sensing data, *Water Resour. Res.*, 37, 329–340, 2001.
- Kite, G. W. and Droogers, P.: Comparing evapotranspiration estimates from satellites, hydrological models and field data, *J. Hydrol.*, 229, 3–18, 2000.
- Kizer, M. A. and Elliott, R. L.: Eddy correlation systems for measuring evapotranspiration, *T. ASAE*, 34, 387–392, 1991.
- Kleissl, J., Gomez, J. D., Hong, S.-H., and Hendrickx, J. M. H.: Large aperture scintillometer intercomparison study, *Bound.-Lay. Meteorol.*, 128, 133–150, 2008.
- Kleissl, J., Hong, S.-H., and Hendrickx, J. M. H.: New Mexico scintillometer network. Supporting remote sensing and hydrologic and meteorological models, *B. Am. Meteorol. Soc.*, 90, 207–218, 2009.
- Kurc, S. A. and Small, E. E.: Dynamics of evapotranspiration in semiarid grassland and shrubland ecosystems during the summer monsoon season, central New Mexico, *Water Resour. Res.*, 40, W09305, doi:10.1029/2004WR003068, 2004.
- Kustas, W. P. and Norman, J. M.: Use of remote sensing for evapotranspiration monitoring over land surfaces, *Hydrolog. Sci. J.*, 41, 495–516, 1996.
- Kustas, W. P., Prueger, J. H., Hatfield, J. L., Ramalingam, K., and Hipps, L. E.: Variability in soil heat flux from a mesquite dune site, *Agr. Forest Meteorol.*, 103, 249–264, 2000.
- Loescher, H. W., Ocheltree, T., Tanner, B., Swiatek, E., Dano, B., Wong, J., Zimmerman, G., Campbell, J., Stock, C., Jacobsen, L., Shiga, Y., Kollas, J., Liburdy, J., and Law, B. E.: Comparison of temperature and wind statistics in contrasting environments among different sonic anemometer-thermometers, *Agr. Forest Meteorol.*, 133, 119–139, 2005.

13515

- Ma, Y., Menenti, M., Tsukamoto, O., Ishikawa, H., Wang, J., and Gao, Q.: Remote sensing parameterization of regional land surface heat fluxes over arid area in northwestern China, *J. Arid Environ.*, 57, 257–273, 2004.
- Moran, M. S. and Jackson, R. B.: Assessing the spatial distribution of evapotranspiration using remotely sensed inputs, *J. Environ. Qual.*, 20, 725–735, 1991.
- Mu, Q., Zhao, M., and Running, S. W.: Improvements to a MODIS global terrestrial evapotranspiration algorithm, *Remote Sens. Environ.*, 115, 1781–1800, 2011.
- Norman, J. M., Kustas, W. P., and Humes, K. S.: A two-source approach for estimating soil and vegetation energy fluxes from observations of directional radiometric surface temperature, *Agr. Forest Meteorol.*, 77, 263–293, 1995.
- Norman, J. M., Anderson, M. C., Kustas, W. P., French, A. N., Mecikalski, J., Torn, R., Diak, G. R., Schmugge, T. J., and Tanner, B. C. W.: Remote sensing of surface energy fluxes at 10<sup>1</sup>-m pixel resolutions, *Water Resour. Res.*, 39, 1221, doi:10.1029/2002WR001775, 2003.
- Parlange, M. B., Eichinger, W. E., and Albertson, J. D.: Regional scale evaporation and the atmosphere boundary layer, *Rev. Geophys.*, 33, 99–124, 1995.
- Paw, K. T., Wharton, S., Xu, L., Falk, M., Schroeder, M., and Gonzales, E.: Zen and the art of energy balance closure, Symposium “Progress in Radiation and Energy Balance Closure”, 68th Annual Meeting Soil Science Society of America, Seattle, Washington, 31 October–4 November 2004.
- Pelgrum, H. and Bastiaanssen, W. G. M.: An intercomparison of techniques to determine the area-averaged latent heat flux from individual in situ observations: a remote sensing approach using the European Field Experiment in a Desertification-Threatened Area data, *Water Resour. Res.*, 32, 2775–2786, 1996.
- Peters Lidard, C. D., Kumar, S., Tian, Y., Eastman, J. L., and Houser, P.: Global urban-scale land-atmosphere modeling with the land information system, 84th AMS Annual Meeting, Symposium on Planning, Nowcasting, and Forecasting in the Urban Zone, 84th AMS Annual Meeting, 11–15 January 2004, Seattle, Washington, 2004.
- Sauer, T. J.: Soil heat flux, in: *Encyclopedia of Soil Science*, edited by: Lal, R., Marcel Dekker Inc., New York, NY, 647–649, 2002a.
- Sauer, T. J.: Heat flux density, in: *Methods of Soil Analysis. Part 1*, edited by: Dane, J. and Topp, C., Soil Science Society of America Madison, Wisconsin, 1233–1248, 2002b.

13516

- Sauer, T. J., Meek, D. W., Ochsner, T. E., Harris, A. R., and Horton, R.: Errors in heat flux measurement by flux plates of contrasting design and thermal conductivity, *Vadose Zone J.*, 2, 580–588, 2003.
- Schmid, H. P. and Oke, T. R.: A model to estimation the source area contributing to turbulent exchange in the surface layer over patchy terrain, *Q. J. Roy. Meteor. Soc.*, 116, 965–988, 1990.
- Schuepp, P. H., Leclerc, M. Y., MacPherson, J. I., and Desjardins, R. L.: Footprint prediction of scalar fluxes from analytical solutions of the diffusion equation, *Bound.-Lay. Meteorol.*, 50, 355–373, 1990.
- Schüttemeyer, D., Schillings, C., Moene, A. F., and Bruin, H. A. R. D.: Satellite-based actual evapotranspiration over drying semiarid terrain in West Africa, *J. Appl. Meteorol. Clim.*, 46, 97–111 doi:10.1175/JAM2444.1, 2007.
- Scott, R. L., Shuttleworth, J. W., Goodrich, D. C., and Maddock III, T.: The water use of two dominant vegetation communities in a semiarid riparian ecosystem, *Agr. Forest Meteorol.*, 105, 241–256, 2000.
- Scott, R. L., Edwards, E. A., Shuttleworth, W. J., Huxman, T. E., Watts, C., and Goodrich, D. C.: Interannual and seasonal variation in fluxes of water and carbon dioxide from a riparian woodland ecosystem, *Agr. Forest Meteorol.*, 122, 65–84, 2004.
- Seguin, B. D. and Itier, B.: Using midday surface temperature to estimate daily evapotranspiration from satellite thermal IR data, *Int. J. Remote Sens.*, 4, 371–383, 1983.
- Senay, G. B., Bohms, S., Singh, R. K., Gowda, P. H., Velpuri, N. M., Alemu, H., and Verdin, J. P.: Operational evapotranspiration mapping using remote sensing and weather datasets: a new parameterization for the SSEB approach, *J. Am. Water Resour. As.*, 49, 577–591, 2013.
- Stannard, D. I.: Comparison of Penman–Monteith, Shuttleworth–Wallace, and Modified Priestley–Taylor evapotranspiration models for wildland vegetation in semiarid rangeland, *Water Resour. Res.*, 29, 1379–1392, 1993.
- Steinwand, A. L., Harrington, R. F., and Or, D.: Water balance for Great Basin phreatophytes derived from eddy covariance, soil water, and water table measurements, *J. Hydrol.*, 329, 595–605, 2006.
- Stromberg, J. C.: Dynamics of Fremont cottonwood (*Populus fremontii*) and saltcedar (*Tamarix chinensis*) populations along the San Pedro River, Arizona, *J. Arid Environ.*, 40, 133–155, 1998.

13517

- Su, Z.: The Surface Energy Balance System (SEBS) for estimation of turbulent heat fluxes, *Hydrol. Earth Syst. Sci.*, 6, 85–100, doi:10.5194/hess-6-85-2002, 2002.
- Sugita, M. and Brutsaert, W.: Daily evaporation over a region from lower boundary layer profiles measured with radiosondes, *Water Resour. Res.*, 27, 747–752, 1991.
- Sumner, D. M. and Jacobs, J. M.: Utility of Penman–Monteith, Priestley–Taylor, reference evapotranspiration, and pan evaporation methods to estimate pasture evapotranspiration, *J. Hydrol.*, 308, 81–104, 2005.
- Tasumi, M.: Progress in operational estimation of regional evapotranspiration using satellite imagery, PhD thesis, University of Idaho, Moscow, Idaho, 2003.
- Teixeira, A. H. C., Bastiaanssen, W. G. M., Moura, M. S. B., Soares, J. M., Ahmad, M. D., and Bos, M. G.: Energy and water balance measurements for water productivity analysis in irrigated mango trees, Northeast Brazil, *Agr. Forest Meteorol.*, 148, 1524–1537, 2008.
- Trezza, R.: Evapotranspiration using a satellite-based surface energy balance with standardized ground control. Ph.D. thesis, Utah State University, Logan, Utah, 2002.
- Twine, T. E., Kustas, W. P., Norman, J. M., Cook, D. R., Houser, P. R., Meyers, T. P., Prueger, J. H., Starks, P. J., and Wesely, M. L.: Correcting eddy-covariance flux underestimates over a grassland, *Agr. Forest Meteorol.*, 103, 279–300, 2000.
- Wang, J., Bastiaanssen, W. G. M., Ma, Y., and Pelgrum, H.: Aggregation of land surface parameters in the oasis-desert systems of Northwest China, *Hydrol. Process.*, 12, 2133–2147, 1998.
- Willmott, C. J.: On the validation of models, *Phys. Geogr.*, 2, 184–194, 1981.
- Willmott, C. J.: Some comments on the evaluation of model performance, *B. Am. Meteorol. Soc.*, 63, 1309–1313, 1982.
- Willmott, C. J. and Wicks, D. E.: An empirical method for the spatial interpolation of monthly precipitation within California, *Phys. Geogr.*, 1, 59–73, 1980.
- Wright, J. L.: New evapotranspiration crop coefficients, *J. Irrig. Drain. E.-ASCE*, 108, 57–74, 1982.
- Yang, Y. T. and Shang, S. H.: A hybrid dual source scheme and trapezoid framework based evapotranspiration model (HTEM) using satellite images: algorithm and model test, *J. Geophys. Res.*, 118, 2284–2300, 2013.
- Zwart, S. J. and Leclert, L. M. C.: A remote sensing-based irrigation performance assessment: a case study of the Office du Niger in Mali, *Irrigation Sci.*, 28, 371–385, 2010.

13518











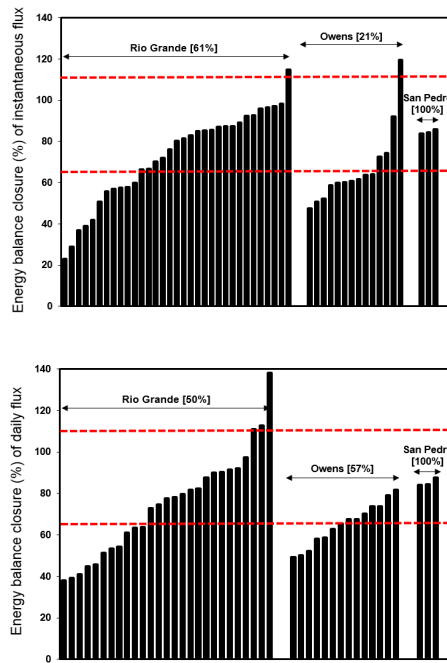


**Figure 1.** Distribution of energy balance relative closure  $(H + LE)/(R_n - G)$  of instantaneous (top panel) and total daily (bottom panel) fluxes from eddy covariance towers. Each “bar” represents a satellite overpass day. The dotted lines show criteria of acceptable closure (65 and 110%) and percentage of the data having acceptable closure is shown in bracket.

13527

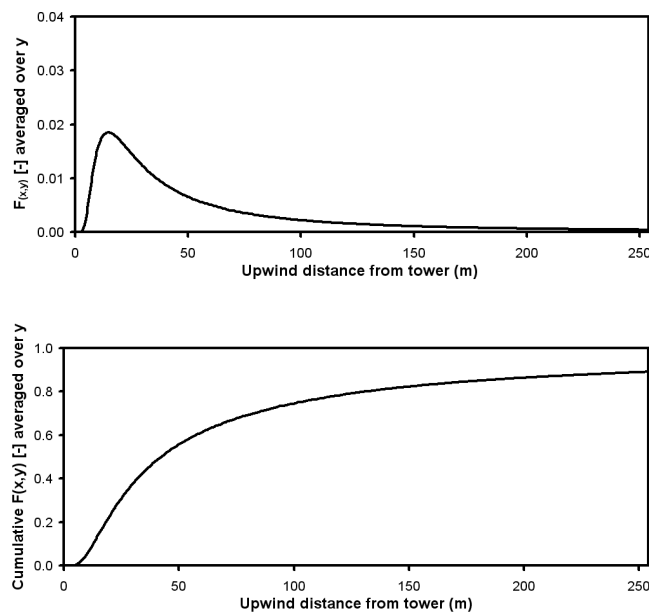


**Figure 2.** Footprint size and footprint intensity from the eddy covariance tower located at SEV (saltcedar) in Rio Grande on 19 August 2002 (10:40 a.m.) (wind speed:  $3.4 \text{ ms}^{-1}$ , vegetation height: 4.9 m and sonic anemometer height from ground: 6.5 m).

13528

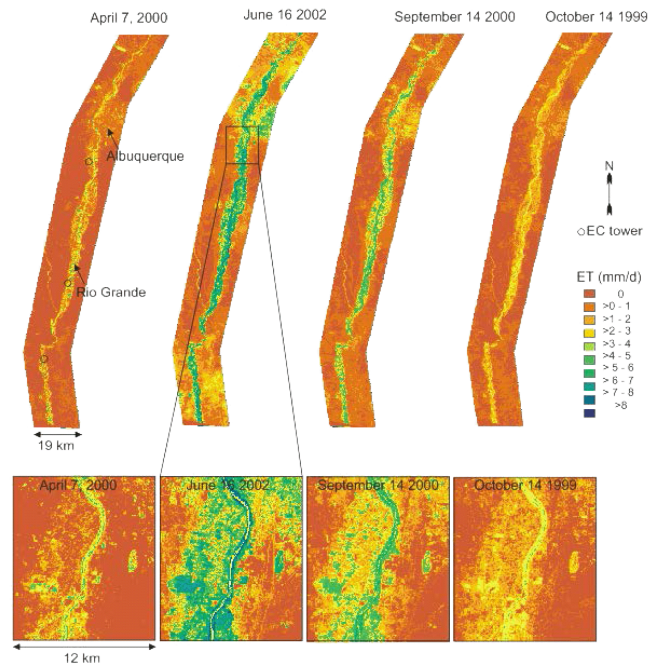


**Figure 3.** SEBAL daily evapotranspiration ( $\text{mm day}^{-1}$ ) maps along the Rio Grande in spring, summer and fall.

13529

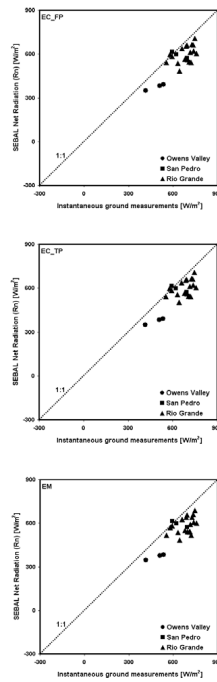


**Figure 4.** Comparison of instantaneous net radiation ( $R_n$ ) between net radiometer measurements and SEBAL estimates. EC\_FP (S1) method selected anchor pixels to match fluxes of the ground measured instantaneous LE (adjusted for closure error) at the satellite overpass and the footprint weight averaged SEBAL LE. EC\_TP (S2) method selected anchor pixels to match fluxes of the ground measured instantaneous LE and the flux of the tower pixel. EM (S3) method selected the anchor pixels with the hydrogeological features of the landscape and micrometeorological considerations.

13530

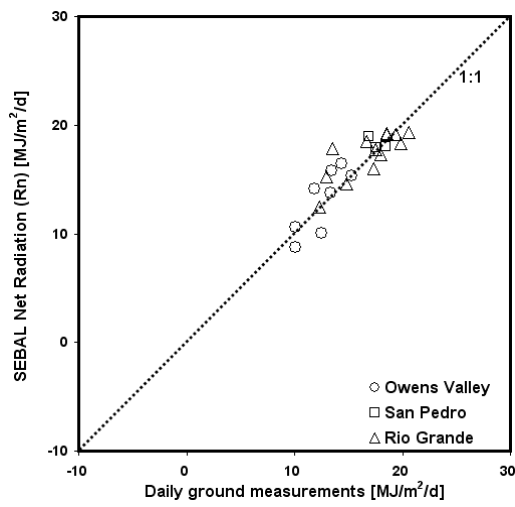


**Figure 5.** Comparison of daily net radiation ( $R_n$ ) between net radiometer measurements and SEBAL estimates.

13531

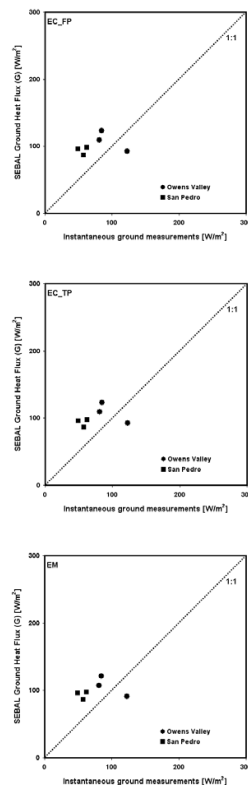


**Figure 6.** Comparison of instantaneous ground heat flux ( $G$ ) between soil heat flux plate measurements and SEBAL estimates in Owens Valley and San Pedro Valley.

13532

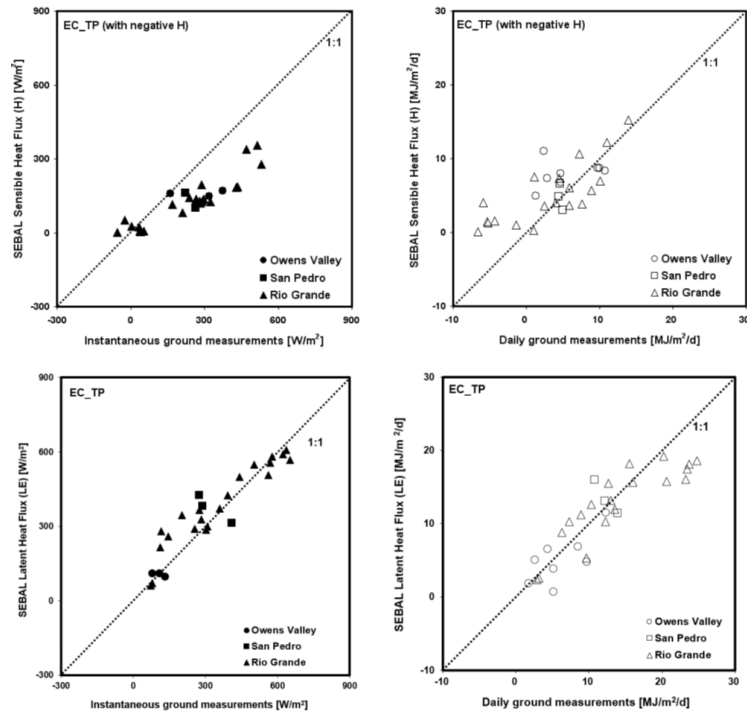


**Figure 7.** Comparison of sensible ( $H$ ) and latent heat ( $LE$ ) fluxes between adjusted eddy covariance tower measurements and SEBAL estimates from scenario S2 (EC\_TP).

13533

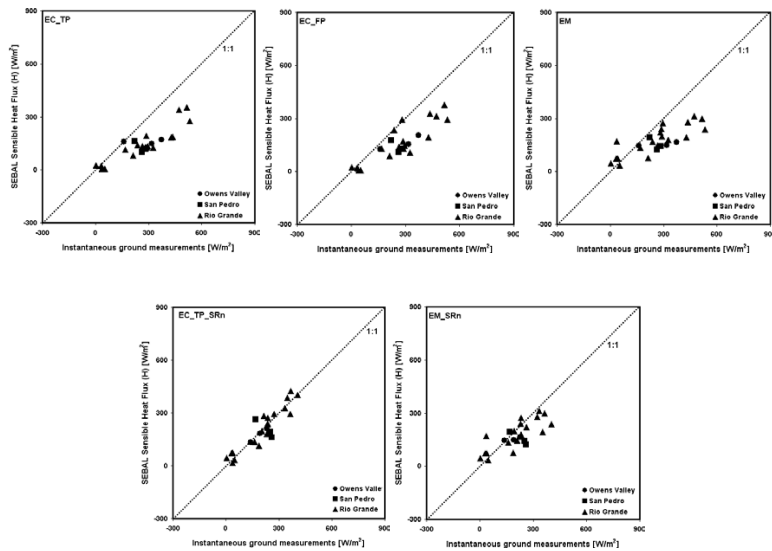


**Figure 8.** Comparison of instantaneous sensible heat flux ( $H$ ) between adjusted eddy covariance tower measurements and SEBAL estimates for scenarios S1–S5.

13534

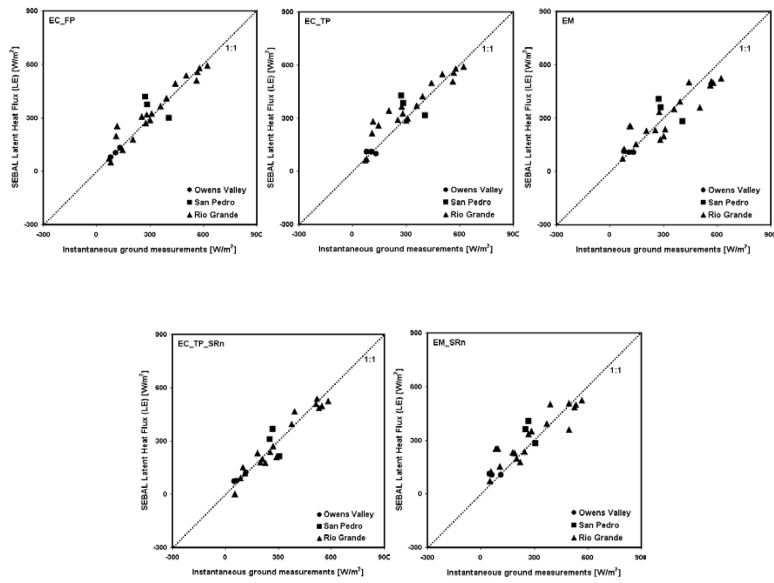


**Figure 9.** Comparison of instantaneous latent heat flux (LE) between adjusted eddy covariance tower measurements and SEBAL estimates for scenarios S1–S5.

13535

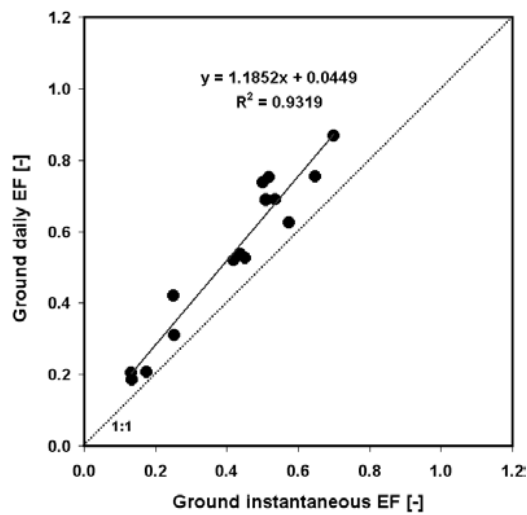


**Figure 10.** Comparison of satellite overpass instantaneous evaporative fraction (EF) with day-time average measured on the ground.

13536

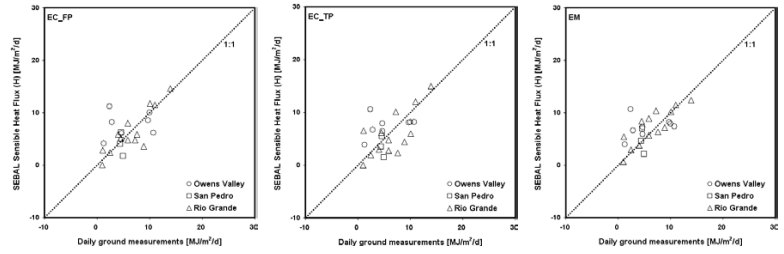


**Figure 11.** Comparison of daily sensible heat flux ( $H$ ) between adjusted eddy covariance tower measurements and SEBAL estimates ( $EF_{24} = 1.1 \times EF_{inst}$ ).

13537

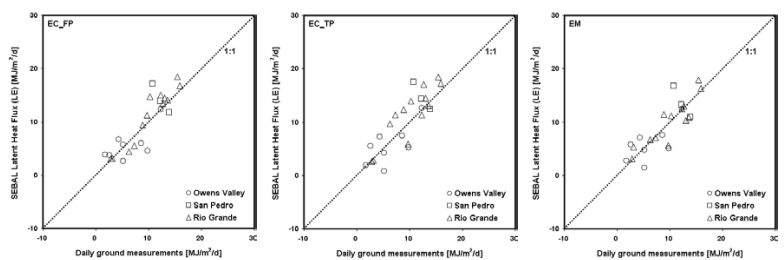


**Figure 12.** Comparison of daily latent heat flux ( $LE$ ) between adjusted eddy covariance tower measurements and SEBAL estimates ( $EF_{24} = 1.1 \times EF_{inst}$ ).

13538

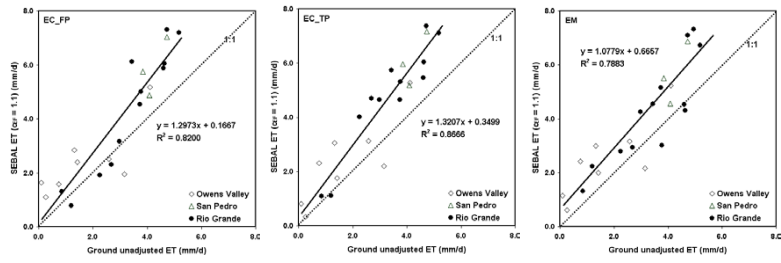


**Figure 13.** Comparison of ET rates determined from SEBAL with  $c_{EF}$  of 1.1 to eddy covariance ground measurements in riparian areas of the Rio Grande Valley (NM), San Pedro Valley (AZ), and Owens Valley (CA).